Chemical Engineering Journal 406 (2021) 127121

Contents lists available at ScienceDirect

Chemical Engineering Journal

journal homepage: www.elsevier.com/locate/cej

Post combustion carbon capture with supported amine sorbents: From adsorbent characterization to process simulation and optimization

Shreenath Krishnamurthy *, Anna Lind, Aud Bouzga, Joanna Pierchala, Richard Blom

Process Chemistry and Functional Materials, SINTEF Industry, Oslo 0373, Norway

ARTICLE INFO

Keywords:
CCS
Supported amine sorbents
CO_2 capture
Vacuum swing adsorption
Process optimization

ABSTRACT

Supported amine sorbents are extensively studied in literature due to their moisture tolerating abilities. Most of the work with this group of adsorbents pertain to experimental studies on adsorption capacity, kinetics, and stability tests on powdered sorbents. Only a handful of published studies have carried out thermodynamic assessment and process modelling to evaluate the performance of supported amine sorbents in the context of pressure and temperature swing adsorption processes. In this work, we have evaluated a commercially available mesoporous silica (PERLKAT) adsorbent grafted with N-[3-(trimethoxysilyl)propyl] ethylenediamine for post-combustion carbon capture by vacuum swing adsorption process (VSA). Experiments were first carried out to obtain information on single component and ternary equilibrium data. The adsorbent has a total capacity of 0.95 mmol/g at 0.15 bar CO_2 and 0.8 mmol/g at 0.05 bar CO_2 respectively at 70 °C. Ternary experiments at low relative humidity shows that the CO_2 capacity is not affected in the presence of moisture. These results were used as input to simulate and optimize a 6-step dual reflux vacuum swing adsorption (VSA) cycle. Detailed process optimization shows that it is possible to capture 90% of the CO_2 at 95% purity using our adsorbent. The minimum specific energy is 1 MJ/kg CO_2 captured on an electric basis when the VSA process is operated at 90 °C.

1. Introduction

Emissions from fossil fuel combustion and industrial sources account for about 78% increase in greenhouse gas emissions since 1970s and about a quarter of the global CO_2 emissions come from large point sources such as power plants that use fossil fuels for generating electricity [1]. There are three major technologies for capturing CO_2 from power plants: 1) pre-combustion carbon capture technology, where the CO_2 capture occurs before fuel combustion, 2) post-combustion carbon capture technology, where the CO_2 capture occurs after burning the fuel and 3) oxy-fuel combustion in which the fuel is burnt in the presence of oxygen. For existing power plants, post combustion carbon capture technology is the most suitable since the capture unit can be retrofitted to the power plant.

Absorptive CO_2 capture using amines is the current benchmark process for carbon capture, but its drawback is the high energy requirement for regeneration of amines. Therefore, extensive research is being carried out to evaluate absorption process [2–4], membranes [5,6] and adsorption separation processes, as potential candidates for capturing and concentrating CO_2 from these sources [7–12]. In the case of adsorption processes, the research is mainly focused on the development of novel materials, such as metal organic frameworks (MOFs), zeolite imidazolate frameworks (ZIFs) and covalent organic frameworks (COFs) with high CO_2 selectivity and capacity [13–15], and process design and optimization to identify optimal process configuration and operating conditions [7,10,16].

A typical post-combustion flue gas contains 4–15% CO_2, depending on the fuel used, along with a large amount of nitrogen and water vapour [17–19]. One of the key challenges in implementing adsorption-based carbon capture technologies is the presence of large amounts of moisture in the flue gas, which is known to be detrimental to CO_2 adsorption. For instance in the case of zeolites, the H_2O competes with CO_2, and for most MOFs, the stability in the presence of moisture may be an issue [20–25]. Supported amine sorbents with good CO_2 adsorption capacity and moisture tolerance can be potential adsorbents for CO_2 capture [26,27]. The supported amine sorbents are prepared by impregnating or grafting a mesoporous silica or an activated carbon with various amines.

There are various studies on functionalizing silica, carbon and metal organic frameworks (MOFs) with different amines, such as polyethyleneimine (PEI) [27–32], tetraethylenepentamine (TEPA) [33–38],

* Corresponding author.
E-mail address: Shreenath.Krishnamurthy@sintef.no (S. Krishnamurthy).

https://doi.org/10.1016/j.cej.2020.127121
Received 9 March 2020; Received in revised form 26 August 2020; Accepted 20 September 2020
Available online 24 September 2020

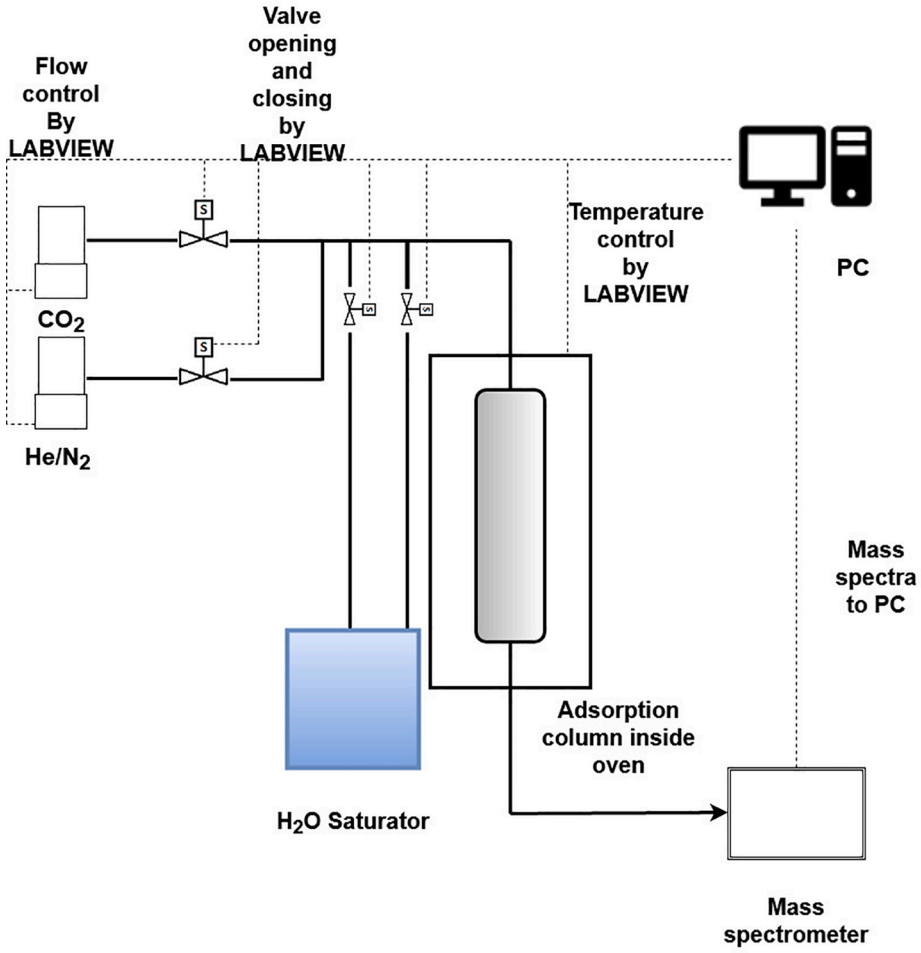

Fig. 1. Schematic of the breakthrough set up used in our study.

benzyl amine [39], various amino silanes [31,34,40,41] and other amino groups [26,42,43], either by grafting or impregnation,. PEI is commonly used, and most of the studies use silicas such as SBA-15 and MCM-41 as substrates, with a few studies using commercially available mesoporous silica. The variations in the silica substrate and the amines used have resulted in a range of CO_2 capacities at post combustion flue gas conditions. For instance, SBA-15 silica impregnated with PEI had a capacity of around 2.4–2.9 at 75 °C, while a TEPA impregnated SBA-15 exhibited a CO_2 capacity of 3.5 mmol/g at 0.1 bar at the same temperature [44]. Amino silanes exhibited a range of capacities from around 0.5–2 mmol/g. MCM-41 silica impregnated with PEI had a CO_2 capacity of around 2 mmol/g [44]. A study on a Mg-MOF-74 grafted with TEPA revealed that amine grafting enhanced the CO_2 capacity at 0.15 bar and 60 °C from 2.67 to 6.02 mmol/g. In the presence of moisture, the adsorbent exhibited an increase in capacity to about 8 mmol/g [37].

There are few studies in the literature that have evaluated the performance of supported amine sorbents in the context of cyclic adsorption processes. Most of these studies are in the context of temperature swing adsorption processes (TSA) in packed and fluidized beds for CO_2 capture [45–50]. A major drawback with the TSA process is that it is associated with long heating and cooling times, which could affect the productivity. The other alternative is a pressure swing adsorption process that cycles between a high pressure and low pressure and does not have any heating or cooling steps. A PSA process cycling between atmospheric pressure and vacuum is called a vacuum swing adsorption (VSA) process and this is suitable for post-combustion CO_2 capture, as it avoids pressurizing the flue gas with large amounts of nitrogen. To the best of our knowledge, there is only one study from Pai et al [51] on process optimization of a VSA cycle using supported amine sorbents. This study was performed to identify the minimum specific energy and maximum productivity achievable in a 4-step VSA process. They found that supported amine sorbents perform better than zeolite 13X owing to their very low nitrogen adsorption.

In most of the studies reporting CO_2 adsorption isotherms, SBA-15 or MCM-41 mesoporous silica is used in a powdered form. For an actual VSA process, these adsorbents must be available in large quantities in pelletized form. As these silica adsorbents are expensive to make, commercially available mesoporous silicas can be used as substrates for grafting or impregnation of amines.

The objective of this work is to evaluate the performance of an amino silane grafted commercially available silica sorbent in the context of a vacuum swing adsorption (VSA) process. First, the first adsorption isotherms of CO_2, N_2 and H_2O were obtained from a commercial volumetric apparatus. An inhouse breakthrough set up was then used to study adsorption of binary and ternary mixtures of CO_2 and N_2 and CO_2, N_2 and H_2O, respectively. The breakthrough set up was also used to study the sorption kinetics of CO_2. These data were then used to simulate and optimize a 6-step vacuum swing adsorption cycle comprising of adsorption, rinse, co-current evacuation, counter-current evacuation, light reflux, and light product pressurization for CO_2 capture from a representative coal-fired power plant. Detailed optimization of the 6-step VSA cycle was then carried out to identify operating conditions at minimum specific energy and maximum productivity subject to 95% CO_2 purity and 90% CO_2 capture rate targets.

2. Experimental section

2.1. Chemicals and materials

Mesoporous silica (PERLKAT) beads (1–3 mm diameter) were received from BASF. N-[3-(trimethoxysilyl) propyl] ethylenediamine (97% purity) and toluene (≥99.5% purity) were purchased from Sigma-Aldrich. CO_2 and N_2 gases were purchased from AGA (99.999% purity).

2.2. Grafting of amine functionalized groups

The silica beads were functionalized with amine groups using the following grafting method adapted from previous publications [52,53]. The silica support (3.0 g) was dried at 150 °C for 2 h before adding it to a solution of N-[3-(trimethoxysilyl)propyl]ethylenediamine (9 ml) and toluene (75 ml) in a 250 ml round bottom flask under Ar atmosphere. The mixture was stirred at room temperature for 1 h before heating in an oil bath to 85 °C under Ar and reflux and kept under these conditions for 24 h. After that, the round bottom flask was lifted from the oil bath and the mixture was allowed to cool down for 30 min before adding water (0.9 ml). The round bottom flask was again lowered into the oil bath to reach 85 °C, and the reaction continued at this temperature for another 24 h with stirring under Ar atmosphere and reflux. After the reaction, the final material was filtered and washed with toluene before drying at 80 °C overnight.

2.3. BET and pore characterization

Specific surface areas were estimated from N_2 isotherms recorded at liquid nitrogen temperatures (77 K) using the BET formalism. Sample activation was typically carried out overnight at an external pre-treatment unit (BELPREP II vac) at 90 °C under vacuum prior to a short (2 hr) pre-treatment at the BELSORP Mini instrument. Micropore volume was estimated using the t-plot method based on said N_2 isotherm measurements at 77 K, while larger pores were analysed using a Hg-porosimeter (Micromeritics AutoPore IV 9520) operating from 10^{-6} bar to 4140 bar covering the pore diameter range from approximately 360 to 0.003 μm.

2.4. Crushing strength

The crushing strength of the beads was measured by using a Zwick/Roell Z250 universal test machine equipped with 500 N load cell. One bead at a time was placed between the parallel compression plates. The lower compression plate was raised at a rate of 0.2 mm per minute while the force (Newton) was recorded as a function of deformation of the bead in millimeter. The force at the moment when each particle breaks is recorded (TestXpert II) and results for the 3–4 beads are averaged and reported as the average crushing strength.

2.5. Adsorption equilibrium

2.5.1. Single component adsorption isotherms

Single component CO_2, N_2 and H_2O isotherms were measured using a commercial volumetric adsorption apparatus obtained from Belsorp. About 100 mg of sample was packed into a sample cell and regenerated overnight at vacuum and 100 °C. Once regeneration was finished experiments were carried out for three different temperatures 70, 90 and 110 °C for CO_2 and at 70, 80 and 90 °C for H_2O. The experiments were carried up to 1 bar for CO_2 and 0.04 bar for H_2O.

2.5.2. Dynamic column breakthrough experiments

The schematic for the breakthrough experiment is shown in Fig. 1 and has been used to study supported amine adsorbents in an earlier publication [50]. The set up contains an oven, which houses the adsorbent column made of stainless steel, mass flow controllers for different gases and a bubbler for introducing moisture. The adsorbent column was 10 cm long and 0.69 cm in diameter. The column also had a provision for a thermocouple to monitor the temperature inside the column. A humidity probe (Vaisala HMT 310, Accuracy ± 0.6% RH) was kept downstream of the column to monitor the humidity. The mass flow controllers were purchased from Bronkhorst (ELFLOW 0–200 ml/min CO_2, 0–400 ml/min, N_2, accuracy ± 0.1% FS). About 2 g of the beads were packed inside the column. The mass flow controllers were calibrated with the corresponding gases, CO_2 and N_2 prior to the experiments. The transient exit concentration was monitored by a mass spectrometer (ThermoFischer PROLAB). The experiments and the data logging were done by LabVIEW software.

First, the packed column was regenerated in-situ overnight at 100 °C under a nitrogen purge of 100 ml/min, and then cooled to the experimental temperature. Once thermal equilibrium was attained, a step change in CO_2 concentration was introduced (30% CO_2 in N_2). Desorption with pure nitrogen succeeded the adsorption step. These experiments were carried out with 30% CO_2 in N_2 at 70, 80 and 90 °C. The adsorption and desorption steps had a flowrate of 150 ml/min and 35 ml/min respectively.

As seen from Fig. 1, the breakthrough apparatus contains a saturator that was filled with 80 ml water and this was used to perform experiments with moist feed. CO_2 and N_2 gases were bubbled through the saturator and the humid gas was fed to the column. After the sample was saturated, desorption was carried out by purging the column with pure nitrogen at 35 ml/min. The breakthrough apparatus has a humidity probe at the downstream of the column, which recorded the relative humidity with respect to time. These breakthrough experiments were carried out with a feed containing 10% CO_2, 2% H_2O and the rest N_2.

Once the breakthrough experiments were complete, the raw mass spectrometer signal was converted to a normalised concentration (C/C_0) in the following manner

$$\frac{C}{C_0} = \frac{\sigma(t) - \sigma_{min}}{\sigma_{max} - \sigma_{min}} \tag{1}$$

Here, σ is the mass spectrometer signal, subscripts max and min correspond to the maximum values of the signal.

The mol fraction of CO_2 with respect to time can be obtained by

$$y(t) = y_0 \frac{C}{C_0} \tag{2}$$

Here, y_0 is the mol fraction of CO_2 in the feed.

After completion of the breakthrough experiments, the packed column was removed and replaced by a 1/16″ tube fitting and adsorption–desorption experiments were repeated with dry and wet gases. This was done to estimate the adsorption isotherms while accounting for the dead volume in the system. To measure the complete isotherm up to 0.3 bar for the dry experiments and 0.1 bar for the wet experiments, we used the desorption branch of the breakthrough experiment. The isotherms were calculated in the following manner by performing mass balance

$$q^* = \frac{FC_T}{m_{ads}} \left(\int_o^t \frac{\frac{c(t)}{c_0}}{1 - \frac{c(t)}{c_0} y0} \Bigg|_{packed} - \int_o^t \frac{\frac{c(t)}{c_0}}{1 - \frac{c(t)}{c_0} y0} \Bigg|_{blank} \right) \tag{3}$$

In this manner, the complete isotherm was obtained from a single experiment by the integration the desorption curve at various concentration levels.

2.5.3. Adsorption kinetics

The breakthrough apparatus was also used to study the kinetics of CO_2 adsorption in the amine sorbent. The breakthrough experiments conducted at 70, 80 and 90 °C were simultaneously analysed using an adsorption model for packed bed, which will be described in the subsequent section. The residual between the experimental temperature

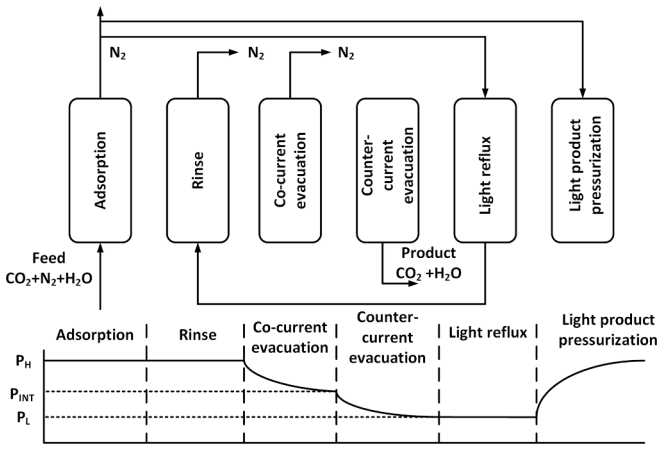

Fig. 2. Schematic of the 6-step VSA cycle with LPP.

Table 1
Input parameters to the adsorption cycle simulation.

Parameter	Value
Length of column (m)	1
Internal diameter (m)	0.1
External diameter (m)	0.11
Column void fraction	0.37
Adsorbent pellet density (kg/m^3)	1052
Adsorbent specific heat (J/kg/K)	1700
Diameter of pellets (mm)	2
Internal heat transfer coefficient (W/m^2 K)	0
External heat transfer coefficient (W/m^2 K)	0
Specific heat of the gas mixture (J/kg/K)	1054
Axial dispersion coefficient (m^2/s)	1.5×10^{-3}
$k_{LDF,\ CO2\ (s^{-1})}$	$10^6 \times e^{-6415/T}$

and concentration curves and the model was minimized by fitting the linear driving force (LDF) coefficient and the heat transfer coefficient values. The objective function for the adsorption step was the following

$$Obj = \sum_{i=1}^{3}\sum_{j=1}^{m}\left(\frac{y_{i,j,sim} - y_{i,j,\ exp}}{y_0}\right)^2 + \sum_{i=1}^{3}\sum_{k=1}^{p}\left(\frac{T_{i,k,\ sim} - T_{i,\ j,exp}}{T_{0,i}}\right)^2 \quad (4)$$

where y and T are the mol fraction and the normalized temperature respectively, the subscripts, sim, exp and 0 stand for simulation, experiment, and feed values, while m and p correspond to the number of experimental points for the concentration and temperature data. For studying the adsorption kinetics, the breakthrough experiments were carried out with a mixture of 15% CO_2 and 85% N_2 as feed.

The simulation of the breakthrough curves was carried out in MATLAB. We have simultaneously fitted the parameters for three temperatures in the adsorption experiments, using a 1-dimensional non-isothermal, non-isobaric model that is well established and validated with experimental data [7,8]. The model is based on the following assumptions:

1. Axial dispersion is considered
2. Ideal gas law is applicable
3. Instantaneous equilibrium between the solid and the gas phases
4. Linear driving force (LDF) approximation to describe the mass transfer
5. Radial gradients in concentration, temperature and pressure are neglected
6. Adsorbent properties and bed voidage are uniform throughout the column
7. The pressure drop is described by Blake-Kozeny equation [54]

The model equations were converted into the non-dimensional form and numerically discretized in the spatial dimension using finite volume technique. Thirty finite volumes and Van-Leer Flux smoothening function were used for discretization [55]. The discretized equations were numerically solved in MATLAB using ode15s solver. Details of the model equations are provided in the Supporting information. The first step was to validate our code by comparing the CO_2 bed profiles from our simulations with the profiles reported in the work of Khurana and Farooq [56].

3. Process study

We have chosen a 6-step cycle with light product pressurization, light reflux, and heavy reflux, as shown in Fig. 2, for this work. This cycle has already been studied by Khurana and Farooq [56] for CO_2 capture from a dry flue gas in post-combustion conditions. The cycle consists of the following steps:

1. **Adsorption with feed**: Here the feed is fed from the bottom of the column (feed end). Preferential adsorption of CO_2 and H_2O occurs inside the column and the light product which is predominantly made up of N_2 is collected at the product end.
2. **Heavy reflux or rinse:** The purpose of this step is to enhance the purity of the CO_2 product. Here, the product stream from the subsequent light reflux step is recycled in its entirety back to the column to enhance the CO_2 concentration in the bed, close to the feed end. This step is carried out at the same pressure as the adsorption step.
3. **Co-current evacuation:** The purpose of this step is to remove the nitrogen from the column and to improve the CO_2 product purity. The column is closed at the feed end, and is evacuated from the product end to an intermediate vacuum pressure (P_{INT}).
4. **Counter-current evacuation**: Here, the column is evacuated from the feed end to a low pressure (P_L) for recovering the CO_2 product. The product end of the column is closed.
5. **Light reflux:** The light reflux step is carried out with a part of the light product from the adsorption step to recover the remaining CO_2 adsorbed in the solid by pulling vacuum from the feed end. The entire stream from the light reflux step is refluxed to the rinse step to conserve the productivity. This stream will have a slightly higher concentration than the feed, but less than that of the counter-current evacuation step. Since the step uses the light product nitrogen from the adsorption step, the duration of this step must be less than the duration of the adsorption step.
6. **Light product pressurization:** The column is pressurized with the remaining light product from the adsorption step to prepare for subsequent feed step.

Table 2
Lower and upper bounds of the decision variables for the optimization.

Variable	Adsorption time (s)	Cocurrent evacuation time (s)	Reflux step time (s)	Counter current evacuation time (s)	Cocurrent evacuation pressure (P_{INT})(bar)	Counter current evacuation pressure (P_L)(bar)	Feed velocity V_0 (m/s)
Lower bound	10	10	1	10	0.1	0.1	0.1
Upper bound	300	300	300	300	0.5	0.5	3

We have considered a system containing 15% CO_2, 5% H_2O and rest N_2 at atmospheric conditions and at feed temperatures of 70 °C and 90 °C. Although the water content in the flue gas at these temperatures is significantly higher than 5%, we have not extrapolated our isotherm data to higher partial pressures to avoid any errors. The presence of oxygen in the flue gas is not considered here. The CO_2 kinetics data were obtained from the dry breakthrough experiments. Nitrogen was considered to be inert and hence a value of 1000 was assigned for the mass transfer coefficient. For water, as an approximation, an equivalent macropore diffusivity (Molecular and Knudsen) was calculated using the mesopore diameter obtained from independent mercury intrusion experiments.

The main performance indicators of the VSA process are CO_2 purity, CO_2 capture rate, specific energy consumption and productivity which are defined as follows

$$CO_2\ \text{Purity} = \frac{\text{Moles}_{CO_2,\text{counter - current evacuation}}}{\text{Moles}_{\text{total,counter - current evacuation}}} \tag{5}$$

$$CO_2\ \text{capture rate} = \frac{\text{Moles}_{CO_2,\text{counter current evacuation}}}{\text{Moles}_{CO_2,\text{fed}}} \tag{6}$$

$$\text{Productivity} = \frac{\text{Moles}_{CO_2,\text{counter current evacuation}}}{\text{Volume of adsorbent x cycle time}} \tag{7}$$

$$\text{Specific energy} = \frac{\text{Energy}_{\text{vacuum}} + \text{Energy}_{\text{compression}}}{\text{Moles}_{CO_2,\text{Counter - current evacuation}}} \tag{8}$$

The energy consumption of the vacuum pumps was calculated using equation 9 given below

$$Energy_{vacuum} = \frac{1}{\eta}\varepsilon_b \pi r_i^2 \frac{\gamma}{\gamma - 1_0} \int_{t=0}^{t=t_{vacuum}} vP\left[\left(\frac{P_{atm}}{P(t)_{vacuum}}\right)^{\frac{\gamma}{\gamma-1}} - 1\right] dt \tag{9}$$

Here ε_b is the bed void fraction, η is the thermodynamic efficiency of the vacuum pump and ϒ is the ratio of the heat capacities. In our simulations, the value of ϒ is 1.4 and we have used a vacuum pump efficiency of 72%.

The simulations were carried out until cyclic steady state was reached, which means that the mass balance error for 5 consecutive cycles was less than 0.6%. The mass balance error is described in the following manner

$$\text{Mass balance error} = \frac{\left|\text{Moles}_{CO_2,in} - \text{Moles}_{CO_2,out}\right|}{\text{Moles}_{CO_2,in}} \text{X } 100 \tag{10}$$

The maximum number of cycles used in the simulations was 300.

3.1. Process optimization

The next step was to perform rigorous process optimization for identifying operating conditions with minimum energy consumption and maximum productivity subject to 95% CO_2 purity and 90% CO_2 capture rate targets. The objective functions are as follows [7,57]

$$\text{Obj}_1 = \frac{\text{Specific Energy}}{100} + 10000 * \max\left(0,\ 0.95 - \frac{CO_2\ \text{purity}}{100}\right)^2 + 10000 * \max\left(0,\ 0.9 - \frac{CO_2\ \text{capture rate}}{100}\right)^2 \tag{11}$$

$$\text{Obj}_2 = \frac{1}{\text{Productivity}} + 10000 * \max\left(0,\ 0.95 - \frac{CO_2\ \text{purity}}{100}\right)^2 + 10000 * \max\left(0,\ 0.9 - \frac{CO_2\ \text{capture rate}}{100}\right)^2 \tag{12}$$

Table 3
Crushing strength values for 4-different pellets.

Sample number	Max crushing strength (N)
1	109
2	75.5
3	113
4	99.5

Here 0.95 and 0.9 correspond to the 95% purity (dry basis) and 90% capture rate constraints. The optimization was carried out using a non-dominated sorting genetic algorithm (NSGA-II) in MATLAB, similar to earlier published studies on VSA cycles [7,10,57]. The input parameters to the process simulator are provided in Table 1. The performance of the VSA cycle is dependent on the feed flowrate, the step durations, and the vacuum pressures. In case of the 6-step cycle the decision variables that affect the performance of the cycle are adsorption step time, the co-current evacuation step time, the counter-current evacuation step time, the reflux step time the co-current evacuation pressure, the counter current evacuation pressure and the feed velocity. The maximum duration of the reflux step was the duration of the adsorption step. The duration of the rinse step was the same as the light reflux step due to the fact that the entire stream is refluxed back into the column. The duration of the light product pressurization step was dependent on the durations of the adsorption and the reflux steps and the light product flowrate. The LPP step was stopped once the high pressure (P_H) was attained as a longer duration does not have any significant impact on the process performance (Table 2.).

The following constraint was imposed to prevent the optimizer from choosing same pressures for co-current and counter-current evacuation steps [7,56]

$$P_{INT} - P_L \geqslant 0.02\ bar \tag{13}$$

4. Results and discussion

4.1. Crushing strength and BET measurements

The crushing strength of four different beads is shown in Table 3. The values vary from 75 to 113 N with the average crushing strength being 99.5 N. The variation in the value is due to expected differences between beads.

The BET measurements using 90 mg of the silica beads showed that the material has a surface area of 117 m^2/g post-grafting while the un-grafted mesoporous silica has a surface area of 328 m^2/g. In comparison the surface area values for SBA-15 and MCM-41 silica are around 550–800 and 1000 m^2/g respectively [58–60].

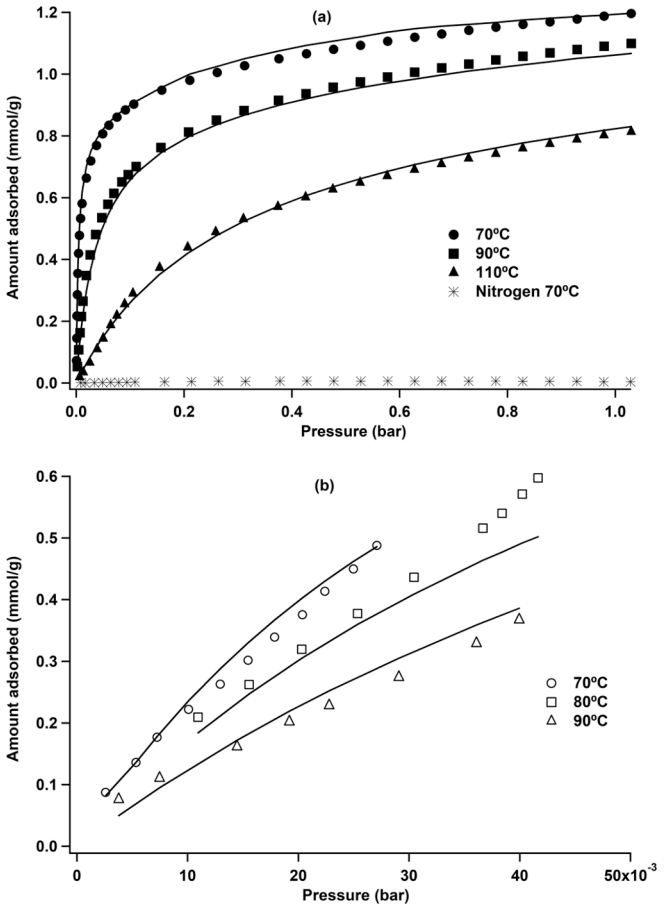

Fig. 3. (a) CO_2 and N_2 and (b) H_2O isotherms obtained from volumetric experiments.

4.2. Volumetric apparatus

Adsorption isotherms of CO_2, N_2 and H_2O are shown in Fig. 3. It can be seen that the nitrogen adsorption is negligible in this sample. The adsorption capacity of CO_2 is 0.95 mmol/g at 0.15 bar and 70 °C. For zeolite 13X, the current benchmark, the value is around 2 mmol/g at the same pressure and temperature in dry conditions [8]. Comparison with other amine grafted sorbents revealed that the CO_2 capacity obtained in our study is in the range of the CO_2 capacity values reported in published literature studies on amino silanes and with those reported by Rezaei et al., on an amino silane grafted silica hollow fibre [31]. Fan et al., on a PEI impregnated silica hollow fiber [61] and Psarras et al., with a pyrrolic group functionalised silica [62]. The CO_2 capacity in our adsorbent is much less than that the values reported for PEI impregnated MCM-41 or SBA-15 mesoporous silica.

The adsorption isotherms of water are linear at the measured range.

Table 4
CO_2 and H_2O adsorption isotherm parameters.

Parameter	Reference pellet	
	CO_2	H_2O
q_{s1}(mmol/g)	0.8	0.8
$b_{0,1}$(bar^{-1})	1.84×10^{-17}	1.85×10^{-5}
ΔH_1 (kJ/mol)	–112.78	–39.8
q_{s2}(mmol/g)	0.5	0.5
$b_{0,2}$(bar^{-1})	1.35×10^{-9}	1.85×10^{-5}
ΔH_2 (kJ/mol)	–49.5	–39.8
ΔH (kJ/mol)	**–111.1**	**–39.8**
K_H 70 °C (mmol/g/bar)	**2.2**	**27.5**
Mean squared error	4.4×10^{-4}	2.2×10^{-4}

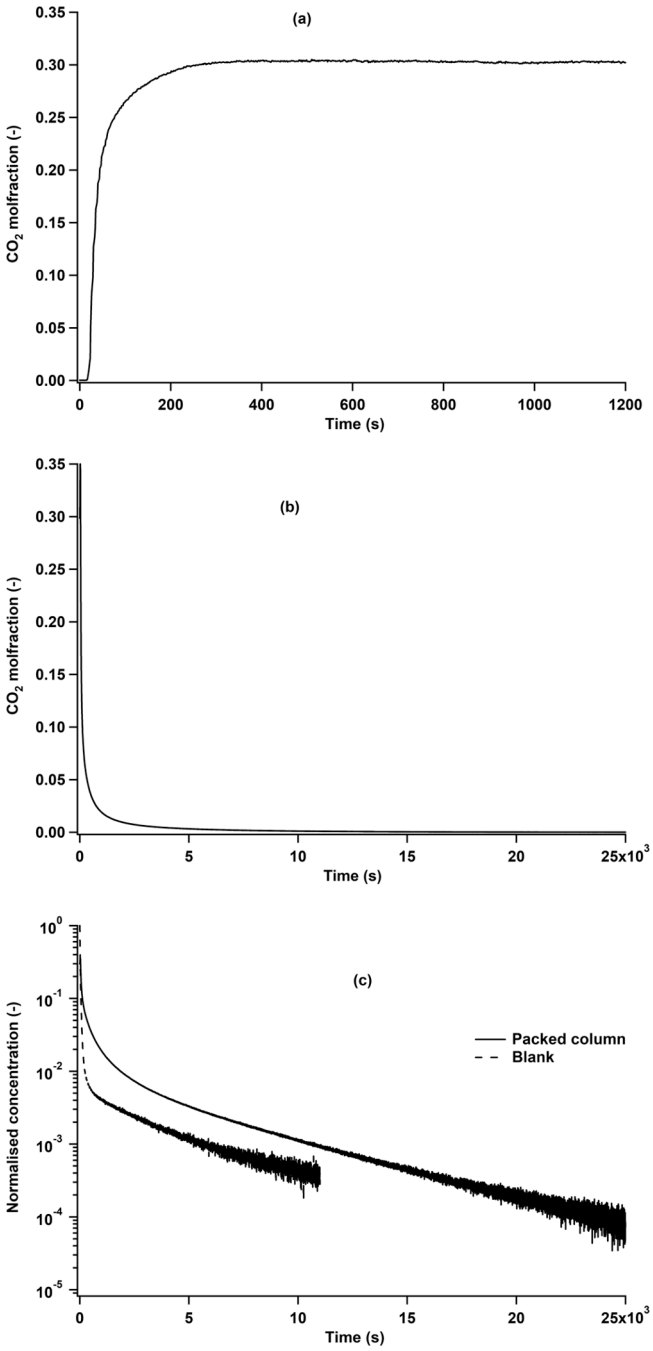

Fig. 4. (a) Adsorption and (b) desorption breakthrough curves at 80 °C. Fig. 4c contains the normalised CO_2 desorption curves for the packed column and the blank.

In this case we were only able to measure the isotherms up to 0.04 bar due to the limitations in our set up.

The isotherm data was fitted to a dual site Langmuir model, which can be expressed as

$$q_i^* = \frac{q_{s1} b_{01} e^{-\Delta\frac{H_1}{RT}} P}{1 + b_{01} e^{-\Delta\frac{H_1}{RT}} P} + \frac{q_{s2} b_{02} e^{-\Delta\frac{H_2}{RT}} P}{1 + b_{02} e^{-\Delta\frac{H_2}{RT}} P} \quad (13)$$

For the sake of consistency, we have kept the saturation capacities for water to be the same as that of CO_2. In general, the fitting is good, except for the higher partial pressures at 80 °C. The dual site Langmuir model may not be the right model to describe H_2O adsorption, nevertheless, the model was able to predict the experimental data. Moreover,

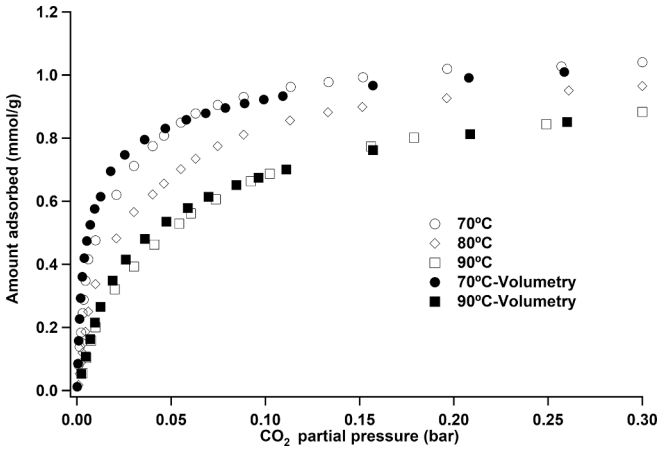

Fig. 5. Comparison of the CO_2 isotherms obtained from the breakthrough experiments and volumetric set up.

Table 5
Comparison of CO_2 capacities obtained from volumetric and breakthrough experiments.

Pressure and temperature	CO_2 capacity from breakthrough experiment (mmol/g)	CO_2 capacity from volumetric experiment (mmol/g)
0.15 bar 70 °C	1.0	0.95
0.15 bar 90 °C	0.78	0.76
0.05 bar 70 °C	0.8	0.8
0.05 bar 90 °C	0.49	0.53

it is straightforward to describe the competitive adsorption with the dual site Langmuir model. The isotherm parameters are provided in Table 4. From the isotherm parameters we can see that the heat of adsorption for CO_2 is around –111 kJ/mol, which is typical of a chemisorption process. This value agrees with the findings of Sanchez-Zambrano et al. [63]. H_2O has a much lower heat of adsorption, which is consistent with literature data [39]. The limiting henry's constant value at reported in Table 4 is obtained from the product of the saturation capacity and the affinity coefficient at 70 °C. For CO_2, the value is 2.2 mmol/g/bar. In comparison, zeolite 13X has a value of 38.2 mmol/g/bar at the same conditions for CO_2 [8].

4.3. Dynamic column breakthrough apparatus

4.3.1. Adsorption equilibrium

Fig. 4 shows the adsorption and desorption curves of CO_2 at 80 °C. The breakthrough of CO_2 is instantaneous with a breakthrough time of 17 s. One can see a slight roll up in the adsorption curve which is related to the temperature effects due to adsorption. Equilibrium with feed concentration is reached in about 10 min. As seen from Fig. 5b, desorption takes longer time than the adsorption and it should be noted that the desorption was carried out at 35 ml/min as opposed to 150 ml/min in adsorption. The desorption is said to be complete if the normalised concentration is 10^{-4} and the base line of the mass spectrometer signal 10^{-10} is achieved. From the normalized CO_2 concentration profile one can see that it takes about 7 h for the completion of the desorption step.

The complete isotherm was obtained using equation 3 shown in the earlier section, using the desorption curves of the blank and the packed columns reported in Fig. 4c. Fig. 5 shows the adsorption isotherms up to 0.3 bar for 70, 80 and 90 °C from the breakthrough experiments. In general, there is a good agreement with the isotherms from the volumetric apparatus. The differences in the shape of the isotherm can be attributed to the differences in the samples used in the two experimental

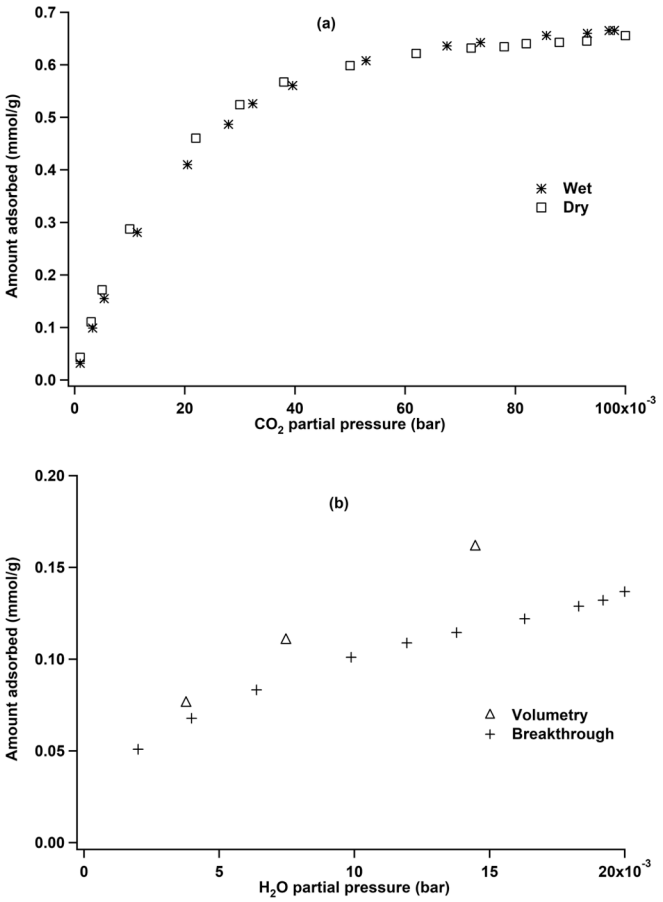

Fig. 6. (a) CO_2 and (b) H_2O isotherms under ternary conditions. The isotherms are from a breakthrough experiment carried out with 10% CO_2 and 2% H_2O in N_2 at 90 °C.

rigs (2 g in the breakthrough experiments vs 100 mg in the volumetric apparatus). We have also calculated partition coefficient used by a few studies to compare different adsorbents and it is defined in the following manner [64,65]

$$\text{Partition coefficient} = \frac{\text{Amount adsorbed}}{\text{partial pressure}} \tag{14}$$

At 0.15 bar, the value was found to be 6.4 mmol/g/bar, and this is about 3 times higher than the henry's constant reported from the volumetric experiments. The value of partition coefficient is slightly lower than a TEPA grafted activated carbon, which has a value of 8.5 mmol/g/bar [64]. Table S1 in the Supporting information provides the raw data for the isotherms obtained from the breakthrough experiments. A comparison of the CO_2 loading at two different partial pressures and temperatures obtained from breakthrough experiments and the volumetric experiments is provided in Table 5.

The CO_2 isotherm under ternary conditions (10% CO_2, 2% N_2 and rest N_2, 90 °C) are shown in Fig. 6. The presence of H_2O in the feed stream did not enhance the adsorption of CO_2 unlike other supported amine sorbents grafted with PEI. We suspect that this could be due to the fact that the water concentration is too low to cause any influence [29,33].On the other hand, CO_2 adsorption is significantly affected in zeolites owing to their strong hydrophilicity. In the work of Cmarik and Knox [66], it was seen that if the zeolite was preloaded with more than 3.6 mol/kg of water, then the CO_2 adsorption capacity becomes negligible.

Using the desorption curve of H_2O, we calculated the ternary adsorption isotherm for H_2O, and we see from Fig. 6 b that there is small drop in the adsorption capacity in comparison to the single component

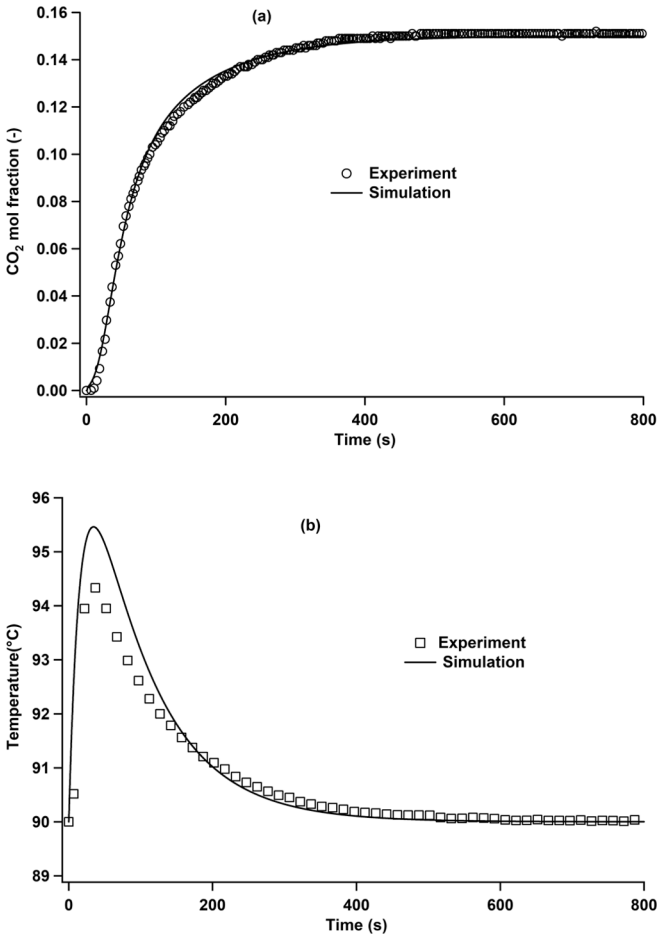

Fig. 7. (a) Concentration and (b) temperature curves in the breakthrough experiment at 90 °C.

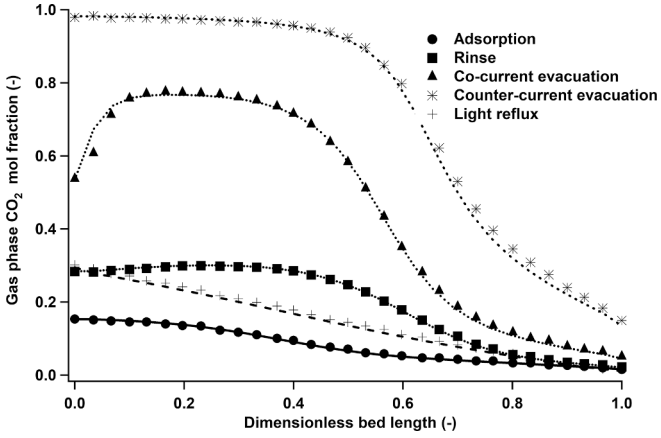

Fig. 8. Validation of our VSA cycle code with the results from Khurana and Farooq. Symbols denote the results from Khurana and Farooq and the lines correspond to our simulated profiles.

isotherms. This could indicate some competition for adsorption between the two gases. As mentioned above, we have used a very low H_2O concentration in the breakthrough experiments. A better understanding of the co-adsorption at high water partial pressures of 10% or more is needed. Performing experiments with a high moisture content may be challenging and molecular simulations can be a good tool to study CO_2-H_2O binary adsorption mechanisms [38,62].

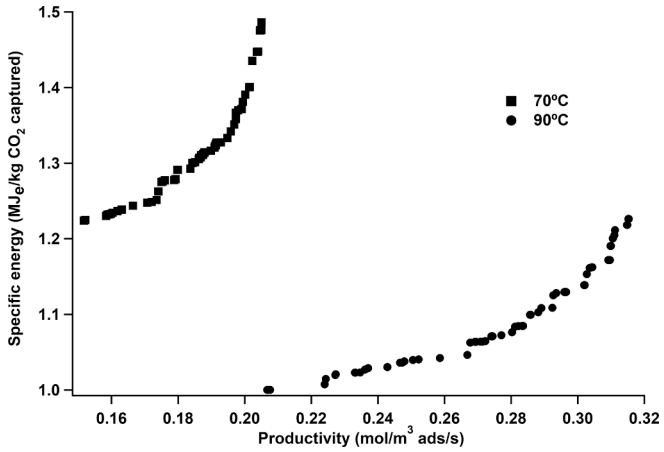

Fig. 9. Specific energy vs productivity pareto fronts for the 6-step VSA process at 70 and 90 °C. The specific energy is on an electric basis.

4.4. Adsorption kinetics

The kinetic constants were obtained by the minimizing the residual between the experiment and simulated concentration and temperature curves simultaneously for experiments carried out at three different temperatures. The temperature dependence of the LDF coefficient was described by the Arrhenius equation. The simulated concentration and temperature curves in the breakthrough experiments are shown in Fig. 7.

4.5. Process study:

In the previous sections, the adsorption capacities at different temperatures and pressures were obtained from two different experimental techniques. Further, we have also reported the henry's constant and the partition coefficient at 0.15 bar and 343 K. These metrics are typically used to compare and rank adsorbents in literature. However, the true ability of the material to achieve the desired process performance targets such as 95% purity and 90% capture rate depend on the specifics of the process configurations. It has been shown in literature that these metrics calculated at constant pressure and temperature conditions do not reflect the conditions in an actual adsorption process [9,10]. Moreover, the performance of these materials is affected by the presence of water and other contaminants as in the case of zeolites and most MOFs [24,25]. Studying the performance of the materials in a cyclic process is therefore a reliable way of assessing the performance of a given adsorbent.

As mentioned before, we have employed a 6-step VSA cycle in this study to evaluate the performance of our amino silane grafted silica. First, we have validated our code with the bed profiles reported in the work of Khurana and Farooq [56]. Fig. 8 shows the CO_2 concentration profiles at cyclic steady state for the different steps of the VSA cycle. It can be seen that there is a very good agreement between the two simulated profiles.

The next step was to carry out detailed process optimization of the 6-step VSA cycle to understand the performance of our supported amine sorbent. We have used the adsorption equilibrium and kinetics data from the volumetric and breakthrough experiments. The breakthrough experiments were conducted with 2% H_2O in the feed due to the limitations in our set up. Therefore, we used the volumetric data measured up to 0.04 bar and extrapolated the competitive effect. The optimization of the VSA cycle was carried out using the gamultiobj, function, which is a part of MATLAB and uses a variant of the NSGA-II algorithm. In total 7000 simulations were performed (50 generations X 140 population per generation) and the trade-off between specific energy and productivity was plotted. Fig. 9 shows the Pareto fronts for the two temperatures, *i.e.*

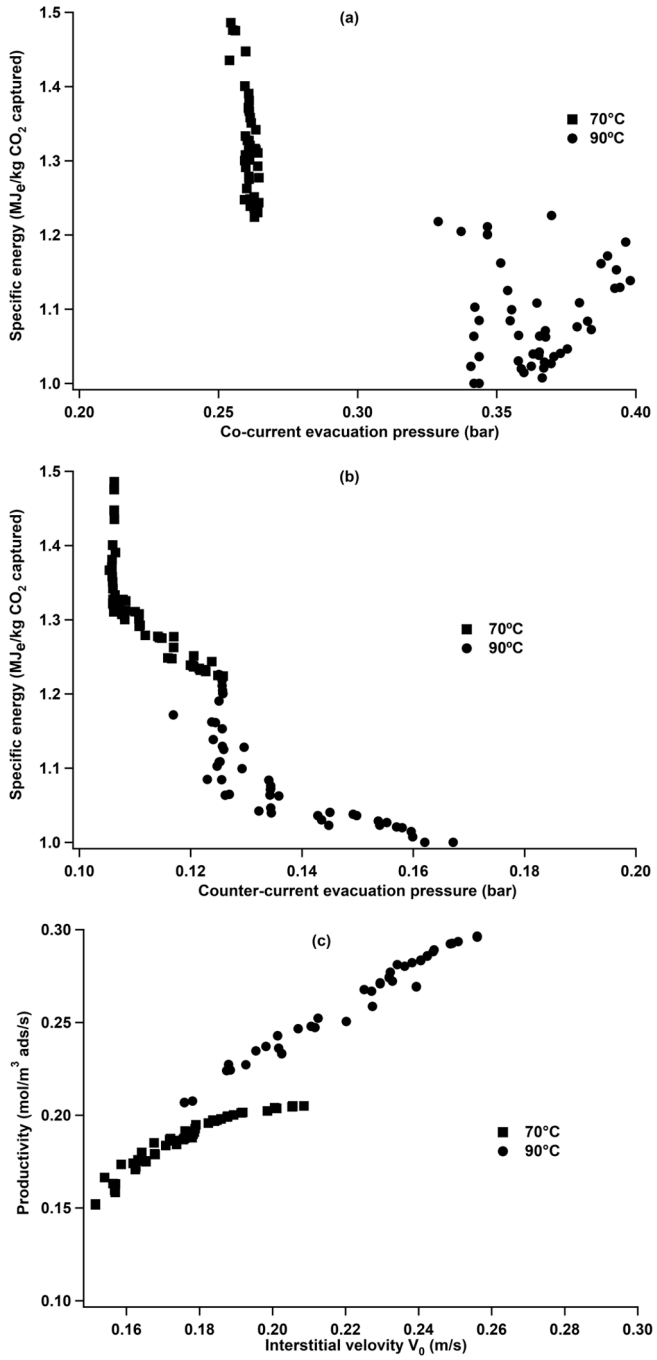

Fig. 10. specific energy vs (a) co-current evacuation pressure (b) counter current evacuation pressure and (c) productivity vs feed velocity. These points correspond to the pareto fronts reported in Fig. 9.

70 and 90 °C, respectively. The specific energy reported here is on an electrical basis. All the points that lie on the Pareto front satisfy 95% purity on a dry basis and 90% capture rate.

As seen from Fig. 9, the adsorption process shows a much better performance at 90 °C than at 70 °C. This can be explained from the plots of the two decision variables, evacuation pressures and flow rate in Fig. 10. At 90 °C the feed velocities are higher than at 70 °C, which led to more moles of CO_2 being treated per cycle and consequently an increase in productivity was observed.

At the higher temperature, the cycle operated with a coarser vacuum in the evacuation steps compared to 70 °C. This is due to the fact that at 70 °C the flowrates are lower and consequently less N_2 is removed in the adsorption and rinse step. So, a deeper vacuum was required in the co-current evacuation step to get rid of the nitrogen. Furthermore, at 70 °C water and CO_2 are adsorbed much stronger, which necessitated a deeper vacuum in the counter-current evacuation step, than at 90 °C. All this resulted in a better performance at the higher temperature.

The minimum specific energy for 70 and 90 °C is 1.22 and 1 MJ/kg, respectively. The maximum productivity values are 0.2 and 0.31 mol/m^3ads/s, respectively. The corresponding operating conditions are provided in Tables 6 and 7. The numbers are closer to the values of 0.27 mol/m^3 ads/s productivity and 0.8 MJ/kg specific energy reported for zeolite 13X, the current reference adsorbent, by Krishnamurthy et al. [57] in a 4-step VSA cycle. Pai et al. [51], reported similar productivity numbers of 0.25–0.4 mol/m^3 ads/s, but much lower energy consumption values of around 0.51–0.63 MJ/kg. However, it should be noted the cycle configuration, feed compositions and operating temperatures in these studies were different and comparison on a similar basis is therefore necessary to benchmark this class of adsorbents with zeolite 13X. The energy performance is comparable with amines like mono-ethanolamine (MEA) which have a specific energy of 1.1–1.4 MJ/kg [67,68] on an electric basis and the sorbent performs slightly better at 90 °C (1.22 and 1 MJ/kg minimum energy at 70 and 90 °C for the 6-step VSA process). However, new amines that show lower energy consumption than MEA process for CO_2 capture are currently in development [69,70]. Therefore, this requires a detailed study on supported amine sorbents via adsorbent ranking in a VSA process and cycle synthesis to identify operating configurations with much lower energy consumption than the MEA process.

Fig. 11 shows the temperature swings in the column for the adsorption and rinse steps corresponding to the feed temperature of 70 and 90 °C. These are the two steps where CO_2 is fed to the column. In both the cases, the maximum temperature values were close to about 120 °C. Such high temperature swings are normally associated with sorbents having high heats of adsorption. Furthermore, the column is also considered adiabatic, which could result in large thermal swings. It has been shown from previous studies that there is a possibility of deterioration in performance if the adsorbent temperature goes beyond 120 °C [31,71]. One can recommend lower feed temperatures to avoid material deterioration, but this can slow down the kinetics and thereby compromising the performance of the VSA process [30]. This necessitates the careful use of these sorbents in the context of a cyclic adsorption process. These large temperature swings also eliminate the need for a temperature swing adsorption process, which would have resulted in a much higher cycle time. A vacuum swing adsorption process with an amine grafted adsorbent exhibiting high CO_2/N_2 selectivity and good moisture tolerance, operating at feed temperatures of 70–90 °C can indeed meet the desired purity and capture rate targets.

5. Conclusions:

In this study we have evaluated a supported amine sorbent in the context of post combustion carbon capture. Single component CO_2 and

Table 6
Operating conditions and performance indicators corresponding to minimum specific energy conditions.

	t_{ads} (s)	$t_{co\text{-}evac}$ (s)	$t_{cn\text{-}evac}$ (s)	t_{reflux} (s)	P_{INT} (bar)	P_L (bar)	V_0 (m/s)	Purity (%)	Capture rate (%)	Prod (mol/m^3/ads/s)	Energy (MJ/kg)
70 °C	68.3	35	48.2	19.1	0.26	0.13	0.15	95	90.5	0.15	1.22
90 °C	89.5	24.7	42.7	22	0.34	0.17	0.18	95.8	90.2	0.21	1.0

Table 7
Operating conditions and performance indicators corresponding to maximum productivity conditions.

	t_{ads} (s)	$t_{co\text{-}evac}$ (s)	$t_{cn\text{-}evac}$ (s)	t_{reflux} (s)	P_{INT} (bar)	P_L (bar)	V_0 (m/s)	Purity (%)	Capture rate (%)	Prod (mol/m^3/ads/s)	Energy (MJ/kg)
70 °C	54.1	26	35.5	18.8	0.25	0.11	0.21	95.1	90.4	0.21	1.49
90 °C	84.5	25.3	34.6	25.2	0.37	0.13	0.27	96	91.1	0.32	1.23

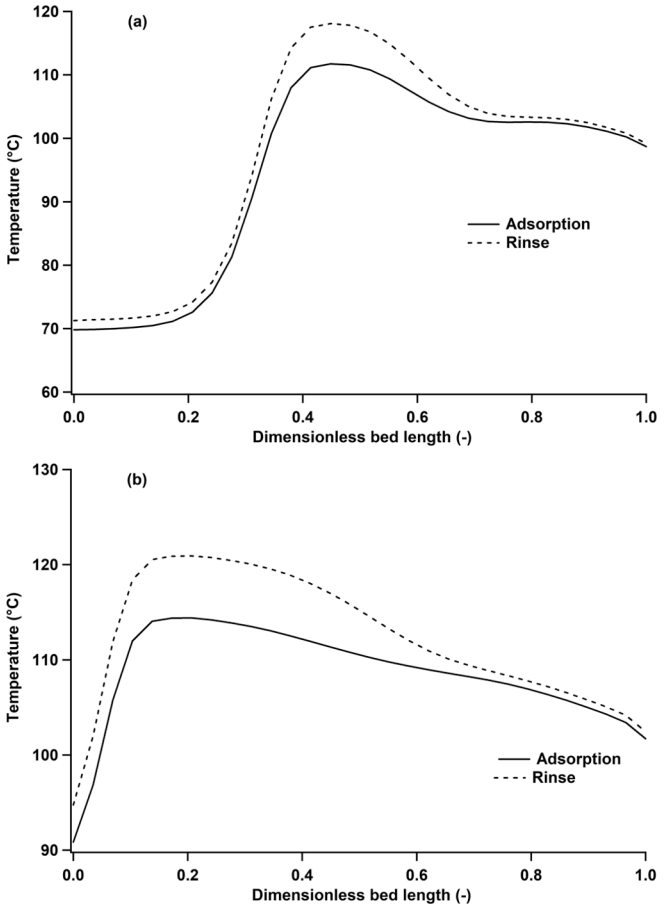

Fig. 11. Temperature profiles at cyclic steady state at the end of adsorption and rinse steps at (a) 70 and (b) 90 °C.

H_2O isotherms were obtained from volumetric experiments performed on a commercial equipment. Dynamic column breakthrough experiments were performed with a 30% CO_2-70% N_2 mixture for three different temperatures (70, 80 and 90 °C). CO_2 isotherms obtained from the breakthrough experiments were in good agreement with the results from the volumetric apparatus. These results also confirmed that N_2 adsorption is negligible in this adsorbent. Ternary breakthrough experiments were then carried out with a 10% CO_2 and 2% H_2O in N_2 as feed at 90 °C. This experiment revealed that at low moisture concentrations, the CO_2 adsorption was not affected. In comparison, adsorbents grafted with PEI show an increase in CO_2 adsorption in the presence of moisture. Nonetheless, unlike zeolites and MOFs, the capacity is not drastically reduced, and this is a positive aspect of our adsorbent. The information from lab scale experiments was used to simulate and optimize a six-step vacuum swing adsorption cycle. With the 6-step cycle it was possible to achieve the purity capture rate targets of 95% and 90% respectively at two feed temperatures of 70 and 90 °C. The adsorbent performed better at the higher temperature owing to less intense vacuum requirements and higher volume of CO_2 treated due to better kinetics. The minimum specific energy at 90 °C was 1 MJ/kg CO_2 captured on an electrical basis and the maximum productivity was 0.31 mol/m^3 ads/s. This work is a basic step to understand the performance of supported amine sorbents in a VSA process. Further work is necessary to understand CO_2 adsorption at high moisture contents and also to identify the optimum operating configurations with energy consumptions comparable to that of the amine-based absorption process with novel solvents.

Declaration of Competing Interest

The authors declare that they have no known competing financial interests or personal relationships that could have appeared to influence the work reported in this paper.

Acknowledgements

This work is a part of the ACT 3D-CAPS project. The ACT 3D-CAPS project has received funding from RCN (Norway, 276322), RVO (The Netherlands, 271503), UEFISCDI, (Romania, 87/2017) and is co-funded by the CO_2 Capture Project (CCP) and the European Commission under the Horizon 2020 programme ACT, Grant Agreement No 691712. The corresponding author would like to acknowledge the discussions with Professor Shamsuzzaman Farooq and Dr Maninder Khurana of National University of Singapore. Discussion with members of the 3D CAPS project is acknowledged. Suggestions from all the anonymous reviewers are acknowledged. The authors would also like to acknowledge Marius Johansen of SINTEF Industry for the crushing strength tests. The authors declare no competing financial interest.

Appendix A. Supplementary data

Supplementary data to this article can be found online at https://doi.org/10.1016/j.cej.2020.127121.

References

[1] IPCC, Climate Change 2014: Synthesis Report. Contribution of Working Groups I, II and III to the Fifth Assessment Report of the Intergovernmental Panel on Climate Change, IPCC, Geneva, Switzerland, 2014.
[2] H. Ahn, M. Luberti, Z. Liu, S. Brandani, Process simulation of aqueous MEA plants for post-combustion capture from coal-fired power plants, Enrgy. Proced. 37 (2013) 1523–1531.
[3] G. Manzolini, E. Sanchez Fernandez, S. Rezvani, E. Macchi, E.L.V. Goetheer, T.J. H. Vlugt, Economic assessment of novel amine based CO_2 capture technologies integrated in power plants based on European Benchmarking Task Force methodology, Appl. Energy 138 (2015) 546–558.
[4] S. Kim, H. Shi, J.Y. Lee, CO_2 absorption mechanism in amine solvents and enhancement of CO_2 capture capability in blended amine solvent, Int. J. Greenh. Gas. Con. 45 (2016) 181–188.
[5] B. Belaissaoui, D. Willson, E. Favre, Post–combustion carbon dioxide capture using membrane processes: a sensitivity analysis, Proc. Eng. 44 (2012) 1191–1195.
[6] M.-C. Ferrari, D. Bocciardo, S. Brandani, Integration of multi-stage membrane carbon capture processes to coal-fired power plants using highly permeable polymers, Green Energy Environ. 1 (2016) 211–221.
[7] R. Haghpanah, R. Nilam, A. Rajendran, S. Farooq, I. Karimi, Cycle synthesis and optimization of a VSA process for postcombustion CO_2 capture, AIChE J. 59 (2013).
[8] S. Krishnamurthy, V.R. Rao, S. Guntuka, P. Sharratt, R. Haghpanah, A. Rajendran, M. Amanullah, I.A. Karimi, S. Farooq, CO_2 capture from dry flue gas by vacuum swing adsorption: A pilot plant study, AIChE J. 60 (2014) 1830–1842.
[9] M. Khurana, S. Farooq, Adsorbent screening for postcombustion CO_2 capture: A method relating equilibrium isotherm characteristics to an optimum vacuum swing adsorption process performance, Ind. Eng. Chem. Res. 55 (2016) 2447–2460.
[10] A.K. Rajagopalan, A.M. Avila, A. Rajendran, Do adsorbent screening metrics predict process performance? A process optimisation based study for post-combustion capture of CO_2, Int. J. Greenh. Gas Con. 46 (2016) 76–85.

[11] P.A. Webley, A. Qader, A. Ntiamoah, J. Ling, P. Xiao, Y. Zhai, A new multi-bed vacuum swing adsorption cycle for CO_2 capture from flue gas streams, Enrgy. Proced.. 114 (2017) 2467–2480.

[12] P. Xiao, J. Zhang, P. Webley, G. Li, R. Singh, R. Todd, Capture of CO2 from flue gas streams with zeolite 13X by vacuum-pressure swing adsorption, Adsorption 14 (2008) 575–582.

[13] H. Yang, J.-R. Li, Metal-organic frameworks (MOFs) for CO_2 capture, in: A.-H. Lu, S. Dai (Eds.), Porous Materials for Carbon Dioxide Capture, Springer Berlin Heidelberg, Berlin, Heidelberg, 2014, pp. 79–113.

[14] Y. Zeng, R. Zou, Y. Zhao, Covalent organic frameworks for CO_2 capture, Adv. Mater. 28 (2016) 2855–2873.

[15] A. Phan, C.J. Doonan, F.J. Uribe-Romo, C.B. Knobler, M. O'Keeffe, O.M. Yaghi, Synthesis, structure, and carbon dioxide capture properties of zeolitic imidazolate frameworks, Acc. Chem. Res. 43 (2010) 58–67.

[16] A. Nalaparaju, M. Khurana, S. Farooq, I.A. Karimi, J.W. Jiang, CO_2 capture in cation-exchanged metal–organic frameworks: Holistic modeling from molecular simulation to process optimization, Chem. Eng. Sci. 124 (2015) 70–78.

[17] A. Feng, T. Kim, X. Li, Z. Riaz, J. Wee, R. Shenoi, P. Wilson, Offshore Renewable Energy Powered CO2 Injection: A Small Carbon Footprint Solution, 2011.

[18] I. Aouini, A. Ledoux, L. Estel, S. Mary, Pilot plant studies for CO_2 capture from waste incinerator flue gas using MEA based solvent, Oil Gas Sci. Technol. - Revue de l IFP 69 (2014) 1091–1104.

[19] C. Scholes, M. Ho, D. Wiley, Membrane-cryogenic post-combustion carbon capture of flue gases from NGCC, Technologies 4 (2016) 14.

[20] G. Li, P. Xiao, P. Webley, J. Zhang, R. Singh, M. Marshall, Capture of CO_2 from high humidity flue gas by vacuum swing adsorption with zeolite 13X, Adsorption 14 (2008) 415–422.

[21] J. Zhang, P. Xiao, G. Li, P.A. Webley, Effect of flue gas impurities on CO_2 capture performance from flue gas at coal-fired power stations by vacuum swing adsorption, Enrgy. Proced. 1 (2009) 1115–1122.

[22] J. Liu, A.I. Benin, A.M.B. Furtado, P. Jakubczak, R.R. Willis, M.D. LeVan, Stability effects on CO_2 adsorption for the DOBDC series of metal-organic frameworks, Langmuir 27 (2011) 11451–11456.

[23] A.C. Kizzie, A.G. Wong-Foy, A.J. Matzger, Effect of humidity on the performance of microporous coordination polymers as adsorbents for CO_2 capture, Langmuir 27 (2011) 6368–6373.

[24] Y. Wang, M.D. LeVan, Adsorption equilibrium of binary mixtures of carbon dioxide and water vapor on zeolites 5A and 13X, J. Chem. Eng. Data 55 (2010) 3189–3195.

[25] S. Zuluaga, E.M.A. Fuentes-Fernandez, K. Tan, F. Xu, J. Li, Y.J. Chabal, T. Thonhauser, Understanding and controlling water stability of MOF-74, J. Mater. Chem. A 4 (2016) 5176–5183.

[26] Y. Belmabkhout, R. Serna-Guerrero, A. Sayari, Adsorption of CO_2-containing gas mixtures over amine-bearing pore-expanded MCM-41 silica: application for gas purification, Ind. Eng. Chem. Res. 49 (2010) 359–365.

[27] A. Sayari, Y. Belmabkhout, Stabilization of amine-containing CO_2 adsorbents: dramatic effect of water vapor, J. Am. Chem. Soc. 132 (2010) 6312–6314.

[28] M.K. Aroua, W.M.A.W. Daud, C.Y. Yin, D. Adinata, Adsorption capacities of carbon dioxide, oxygen, nitrogen and methane on carbon molecular basket derived from polyethyleneimine impregnation on microporous palm shell activated carbon, Sep. Purif. Tech. 62 (2008) 609–613.

[29] A.D. Ebner, M.L. Gray, N.G. Chisholm, Q.T. Black, D.D. Mumford, M.A. Nicholson, J.A. Ritter, Suitability of a solid amine sorbent for CO_2 capture by pressure swing adsorption, Ind. Eng. Chem. Res. 50 (2011) 5634–5641.

[30] G. Knowles, P. Webley, Z. Liang, A. Chaffee, Silica/polyethyleneimine composite adsorbent S-PEI for CO_2 capture by vacuum swing adsorption (VSA), in recent advances in post-combustion CO_2 capture, Chemistry (2012) 177–205.

[31] F. Rezaei, R.P. Lively, Y. Labreche, G. Chen, Y. Fan, W.J. Koros, C.W. Jones, Aminosilane-grafted polymer/silica hollow fiber adsorbents for CO_2 capture from flue gas, ACS Appl. Mater. Interfaces 5 (2013) 3921–3931.

[32] A. Abdollahi-Govar, A.D. Ebner, J.A. Ritter, New kinetic model that describes the reversible adsorption and desorption behavior of CO_2 in a solid amine sorbent, Energy Fuels 29 (2015) 4492–4502.

[33] Y. Liu, Q. Ye, M. Shen, J. Shi, J. Chen, H. Pan, Y. Shi, Carbon dioxide capture by functionalized solid amine sorbents with simulated flue gas conditions, Environ. Sci. Tech. 45 (2011) 5710–5716.

[34] G. Zhang, P. Zhao, L. Hao, Y. Xu, H. Cheng, A novel amine double functionalized adsorbent for carbon dioxide capture using original mesoporous silica molecular sieves as support, Sep. Purif. Technol. 209 (2019) 516–527.

[35] Y. Guo, L. Luo, Y. Zheng, T. Zhu, Optimization of CO_2 adsorption on solid-supported amines and thermal regeneration mode comparison, ACS Omega 5 (2020) 9641–9648.

[36] Q. Liu, J. Shi, S. Zheng, M. Tao, Y. He, Y. Shi, Kinetics studies of CO2 adsorption/desorption on amine-functionalized multiwalled carbon nanotubes, Ind. Eng. Chem. Res. 53 (2014) 11677–11683.

[37] Y. Cao, F. Song, Y. Zhao, Q. Zhong, Capture of carbon dioxide from flue gas on TEPA-grafted metal-organic framework Mg2(dobdc), J. Environ. Sci. 25 (2013) 2081–2087.

[38] X. Huang, J. Lu, W. Wang, X. Wei, J. Ding, Experimental and computational investigation of CO_2 capture on amine grafted metal-organic framework NH2-MIL-101, Appl. Surf. Sci. 371 (2016) 307–313.

[39] R. Veneman, N. Frigka, W. Zhao, Z. Li, S. Kersten, W. Brilman, Adsorption of H_2O and CO_2 on supported amine sorbents, Int. J. Greenh. Gas Con. 41 (2015) 268–275.

[40] L. Wang, L. Ma, A. Wang, Q. Liu, T. Zhang, CO_2 adsorption on SBA-15 modified by aminosilane, Chin. J. Catal. 28 (2007) 805–810.

[41] N. Mittal, A. Samanta, P. Sarkar, R. Gupta, Postcombustion CO_2 capture using N-(3-trimethoxysilylpropyl)diethylenetriamine-grafted solid adsorbent, Energy Sci. Eng. 3 (2015) 207–220.

[42] R. Serna-Guerrero, A. Sayari, Modeling adsorption of CO_2 on amine-functionalized mesoporous silica. 2: Kinetics and breakthrough curves, Chem. Eng. J. 161 (2010) 182–190.

[43] S. Choi, T. Watanabe, T.-H. Bae, D.S. Sholl, C.W. Jones, Modification of the Mg/DOBDC MOF with amines to enhance CO_2 adsorption from ultradilute gases, J. Phys. Chem. Lett. 3 (2012) 1136–1141.

[44] T. Gelles, S. Lawson, A.A. Rownaghi, F. Rezaei, Recent advances in development of amine functionalized adsorbents for CO_2 capture, Adsorption 26 (2020) 5–50.

[45] W. Zhang, H. Liu, C. Sun, T.C. Drage, C.E. Snape, Performance of polyethyleneimine–silica adsorbent for post-combustion CO_2 capture in a bubbling fluidized bed, Chem. Eng. J. 251 (2014) 293–303.

[46] W. Zhang, H. Liu, C. Sun, T.C. Drage, C.E. Snape, Capturing CO_2 from ambient air using a polyethyleneimine–silica adsorbent in fluidized beds, Chem. Eng. Sci. 116 (2014) 306–316.

[47] M. Hefti, L. Joss, Z. Bjelobrk, M. Mazzotti, On the potential of phase-change adsorbents for CO2 capture by temperature swing adsorption, Faraday Discuss. 192 (2016) 153–179.

[48] A. Zaabout, M.C. Romano, S. Cloete, A. Giuffrida, J. Morud, P. Chiesa, S. Amini, Thermodynamic assessment of the swing adsorption reactor cluster (SARC) concept for post-combustion CO_2 capture, Int. J. Greenh. Gas Con. 60 (2017) 74–92.

[49] M.J. Bos, V. Kroeze, S. Sutanto, D.W.F. Brilman, Evaluating regeneration options of solid amine sorbent for CO_2 removal, Ind. Eng. Chem. Res. 57 (2018) 11141–11153.

[50] C. Dhoke, S. Cloete, S. Krishnamurthy, H. Seo, I. Luz, M. Soukri, Y.-K. Park, R. Blom, S. Amini, A. Zaabout, Sorbents screening for post-combustion CO_2 capture via combined temperature and pressure swing adsorption, Chem. Eng. J. 380 (2020), 122201.

[51] K.N. Pai, J.D. Baboolal, D.A. Sharp, A. Rajendran, Evaluation of diamine-appended metal-organic frameworks for post-combustion CO_2 capture by vacuum swing adsorption, Sep. Purif. Technol. 211 (2019) 540–550.

[52] P.J.E. Harlick, A. Sayari, Applications of pore-expanded mesoporous silica. 5. Triamine grafted material with exceptional CO_2 dynamic and equilibrium adsorption performance, Ind. Eng. Chem. Res. 46 (2007) 446–458.

[53] G. Qi, L. Fu, E.P. Giannelis, Sponges with covalently tethered amines for high-efficiency carbon capture, Nat. Commun. 5 (2014) 5796.

[54] D. Nikolic, E. Kikkinides, Modelling and optimization of hybrid PSA/membrane separation processes, Adsorption 21 (2015) 283–305.

[55] R. Haghpanah, A. Majumder, R. Nilam, A. Rajendran, S. Farooq, I.A. Karimi, M. Amanullah, Multiobjective optimization of a four-step adsorption process for postcombustion CO_2 capture via finite volume simulation, Ind. Eng. Chem. Res. 52 (2013) 4249–4265.

[56] M. Khurana, S. Farooq, Simulation and optimization of a 6-step dual-reflux VSA cycle for post-combustion CO_2 capture, Chem. Eng. Sci. 152 (2016) 507–515.

[57] S. Krishnamurthy, R. Haghpanah, A. Rajendran, S. Farooq, Simulation and optimization of a dual-adsorbent, two-bed vacuum swing adsorption process for CO_2 capture from wet flue gas, Ind. Eng. Chem. Res. 53 (2014) 14462–14473.

[58] F. Mariano-Neto, J.R. Matos, L.C. Cides da Silva, L.V. Carvalho, K. Scaramuzzi, O. A. Sant'Anna, C.P. Oliveira, M.C.A. Fantini, Physical properties of ordered mesoporous SBA-15 silica as immunological adjuvant, J. Phys. D Appl. Phys. 47 (2014), 425402.

[59] M. Manzano, V. Aina, C.O. Areán, F. Balas, V. Cauda, M. Colilla, M.R. Delgado, M. Vallet-Regí, Studies on MCM-41 mesoporous silica for drug delivery: Effect of particle morphology and amine functionalization, Chem. Eng. J. 137 (2008) 30–37.

[60] M.R. Mello, D. Phanon, G.Q. Silveira, P.L. Llewellyn, C.M. Ronconi, Amine-modified MCM-41 mesoporous silica for carbon dioxide capture, Micropor. Mesopor. Mater. 143 (2011) 174–179.

[61] Y. Fan, Y. Labreche, R.P. Lively, C.W. Jones, W.J. Koros, Dynamic CO_2 adsorption performance of internally cooled silica-supported poly(ethylenimine) hollow fiber sorbents, AIChE J. 60 (2014) 3878–3887.

[62] P. Psarras, J. He, J. Wilcox, Effect of water on the CO_2 adsorption capacity of amine-functionalized carbon sorbents, Ind. Eng. Chem. Res. 56 (2017) 6317–6325.

[63] K.S. Sánchez-Zambrano, L. Lima Duarte, D.A. Soares Maia, E. Vilarrasa-García, M. Bastos-Neto, E. Rodríguez-Castellón, D.C. Silva de Azevedo, CO_2 capture with mesoporous silicas modified with amines by double functionalization: assessment of adsorption/desorption cycles, Materials (Basel) 11 (2018) 887.

[64] M. Al-Wabel, J. Elfaki, A. Usman, Q. Hussain, Y.S. Ok, Performance of dry water- and porous carbon-based sorbents for carbon dioxide capture, Environ. Res. 174 (2019) 69–79.

[65] K.-H. Kim, J.E. Szulejko, N. Raza, V. Kumar, K. Vikrant, D.C.W. Tsang, N.S. Bolan, Y.S. Ok, A. Khan, Identifying the best materials for the removal of airborne toluene based on performance metrics - A critical review, J. Clean. Prod. 241 (2019), 118408.

[66] G.E. Cmarik, J.C. Knox, Co-Adsorption of Carbon Dioxide on Zeolite 13X in the Presence of Preloaded Water, 48th international conference on environmental systems, 2018.

[67] S.-Y. Oh, M. Binns, H. Cho, J.-K. Kim, Energy minimization of MEA-based CO_2 capture process, Appl. Energy 169 (2016) 353–362.

[68] H. Ahn, S.-H. Hong, Y. Zhang, C.-H. Lee, Experimental and simulation study on CO_2 adsorption dynamics of a zeolite 13X column during blowdown and pressurization: implications of scaleup on CO2 capture vacuum swing adsorption cycle, Ind. Eng. Chem. Res. 59 (2020) 6053–6064.

[69] F. Liu, M. Fang, W. Dong, T. Wang, Z. Xia, Q. Wang, Z. Luo, Carbon dioxide absorption in aqueous alkanolamine blends for biphasic solvents screening and evaluation, Appl. Energy 233–234 (2019) 468–477.
[70] S. Yun, S.-Y. Oh, J.-K. Kim, Techno-economic assessment of absorption-based CO2 capture process based on novel solvent for coal-fired power plant, Appl. Energy 268 (2020), 114933.
[71] P. Bollini, S. Choi, J.H. Drese, C.W. Jones, Oxidative degradation of aminosilica adsorbents relevant to postcombustion CO_2 capture, Energy Fuels 25 (2011) 2416–2425.